Inorganic Chemistry

ARTICLE

pubs.acs.org/IC

Structure−Activity Relationship of Photocytotoxic Iron(III) Complexes of Modified Dipyridophenazine Ligands

Sounik Saha,[†] Dibyendu Mallick,[†] Ritankar Majumdar,[‡] Mithun Roy,[†] Rajan R. Dighe,[‡] Eluvathingal D. Jemmis,*[,†,§] and Akhil R. Chakravarty*[,†]

[†]Department of Inorganic and Physical Chemistry and [‡]Department of Molecular Reproduction, Development and Genetics, Indian Institute of Science, Bangalore-560012, India

[§]Indian Institute of Science Education and Research, Thiruvananthapuram, CET Campus, Thiruvananthapuram, 695016, Kerala, India

Supporting Information

ABSTRACT: Iron(III) complexes [FeL(B)] (**1**−**5**) of a tetradentate trianionic phenolate-based ligand (L) and modified dipyridophenazine bases (B), namely, dipyrido-6,7,8,9-tetrahydrophenazine (dpqC in **1**), dipyrido[3,2-*a*:2′,3′-*c*]phenazine-2-carboxylic acid (dppzc in **2**), dipyrido[3,2-*a*:2′,3′-*c*]phenazine-11-sulfonic acid (dppzs in **3**), 7-aminodipyrido[3,2-*a*:2′,3′-*c*]phenazine (dppza in **4**) and benzo[*i*]dipyrido[3,2-*a*:2′,3′-*c*]phenazine (dppn in **5**), have been synthesized and their photocytotoxic properties studied along with their dipyridophenazine analogue (**6**). The complexes have a five electron paramagnetic iron(III) center, and the Fe(III)/Fe(II) redox couple appears at about −0.69 V versus SCE in DMF-0.1 M TBAP. The physicochemical data also suggest that the complexes possess similar structural features as that of its parent complex [FeL(dppz)] with FeO3N3 coordination in a distorted octahedral geometry. The DNA-complex and protein-complex interaction studies have revealed that the complexes interact favorably with the biomolecules, the degree of which depends on the nature of the substituents present on the dipyridophenazine ring. Photocleavage of pUC19 DNA by the complexes has been studied using visible light of 476, 530, and 647 nm wavelengths. Mechanistic investigations with inhibitors show formation of $HO^{\bullet}$ radicals via a photoredox pathway. Photocytotoxicity study of the complexes in HeLa cells has shown that the dppn complex (**5**) is highly active in causing cell death in visible light with sub micromolar IC_{50} value. The effect of substitutions and the planarity of the phenazine moiety on the cellular uptake are quantified by determining the total cellular iron content using the inductively coupled plasma-optical emission spectrometry (ICP-OES) technique. The cellular uptake increases marginally with an increase in the hydrophobicity of the dipyridophenazine ligands whereas complex **3** with dppzs shows very high uptake. Insights into the cell death mechanism by the dppn complex **5**, obtained through DAPI nuclear staining in HeLa cells, reveal a rapid programmed cell death mechanism following photoactivation of complex **5** with visible light. The effect of substituent on the DNA photocleavage activity of the complexes has been rationalized from the theoretical studies.

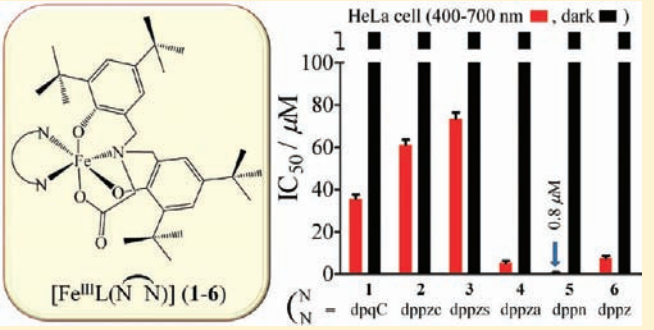

INTRODUCTION

A large number of porphyrin-based compounds have been designed and synthesized to improve the efficacy of the FDA approved photodynamic therapy (PDT) drug Photofrin with the emergence of PDT as a noninvasive treatment modality for tumors.[1,2] This is similar to the efforts of improving the drug activity of cisplatin, the well-known metal-based chemotherapeutic agent.[3] While the peripheral positions of the porphyrin core are modified to circumvent the skin and hepato-toxicity associated with Photofrin, cisplatin is modified using both N- and O-donor ligands targeting both the ammine and the chloride sites to prepare a series of cisplatin analogues that include carboplatin and oxaliplatin. There are also successful efforts toward using platinum(IV) prodrugs to generate active cisplatin species in intracellular medium by reduction of the metal in the presence of a reducing agent or by photochemical means.[4] Quantitative structure−activity relationships thus assume great importance toward enhancing the biological activity of the drug molecule using steric and/or electronic control of the substituent groups in the modified molecule derived from the parent species. This has been done with great success for both Photofrin and cisplatin. It has been observed that porphyrin and other macrocyclic compounds such as benzoporphyrin derivatives,[5] phthalocyanines,[6] ether derivatives of porphyrins,[7] pyropheophorbide-a,[8,9] purpurinimide,[10] and bacteriopurpurinimides[11] exhibit relationships between the hydrophobicity of the molecules and the photodynamic activity. The extent to which a

Received: December 4, 2010
Published: March 10, 2011

Chart 1. Schematic Drawing of the Complexes and the Ligands Used

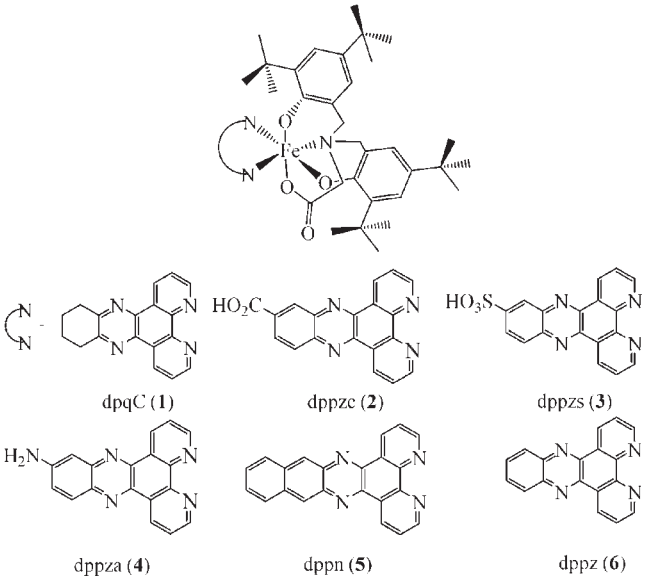

photosensitizer localizes in tumor tissue is determined by the pH gradients, leaky tumor vasculature, and abnormal blood flow contributing to the site and degree of photosensitizer localization.[12,13] It has also been observed that amphiphilic photosensitizers are generally more photodynamically active than symmetrically hydrophilic or hydrophobic molecules.[14,15] Amphiphilicity determines the degree to which a photosensitizer aggregates, which in turn, can affect its photophysical properties.[16] Among the metal-based PDT agents, the structure−activity relationships on various rhodium and ruthenium complexes of polypyridyl ligands have revealed that there exists a strong correlation between the molecular characteristics and their biological activity in vitro.[17,18] Such dependence has been attributed to the ease of membrane permeability and the site of localization of the molecule inside the cell with preference to nucleus or mitochondria or endoplasmic reticulum, and so forth.[17−20] The cellular uptake has been found to be dependent on the size of the polypyridyl ligands and their octanol−water partition coefficients. Therefore, cytotoxicity is exclusively guided by the substituent present on the polypyridyl ligands.

The present work stems from our interest to explore the structure−activity relationship in a series ternary iron(III) complexes having modified dipyridophenazine ligands. This work originates from our recent report of an iron-based potent photochemotherapeutic agent, namely, the dipyridophenazine iron(III) complex [Fe(L)(dppz)] of a trianionic tetradentate phenolate-based ligand (L) exhibiting significantly high photocytotoxicity (IC_{50} = 3.59 μM) upon irradiation with visible light in HeLa cells.[21] In our attempt to investigate the effect of modified dppz ligands with variable lipophilicity to PDT efficacy, we have synthesized iron(III) complexes with various substituents using $-NH_2$ group as electron donating, $-SO_3H$ and $-CO_2H$ groups as electron-withdrawing, extended phenyl ring with an increased aromatic surface area, and dearomatization of the terminal ring by reducing the aromatic surface area on the dipyridophenazine ring. Herein, we present the iron(III) complexes [FeL(B)] (**1**−**5**), where B is a modified dipyridophenazine base, namely, dipyrido-6,7,8,9-tetrahydrophenazine (dpqC in **1**), dipyrido[3,2-*a*:2′,3′-*c*]phenazine-2-carboxylic acid (dppzc in **2**), dipyrido[3,2-*a*:2′,3′-*c*]phenazine-11-sulfonic acid (dppzs in **3**), 7-aminodipyrido[3,2-*a*:2′,3′-*c*]phenazine (dppza in **4**), and benzo[*i*]dipyrido[3,2-*a*:2′,3′-*c*]phenazine (dppn in **5**) (Chart 1). The dppz complex [FeL(dppz)] (**6**) is used as the reference species (dppz, dipyrido[3,2-*a*:2′,3′-*c*]phenazine).[21] The present work describes the *in vitro* photosensitizing activity of the new iron(III)-based photosensitizers. The complexes are also investigated for their DNA and bovine serum albumin (BSA) binding affinity, photonuclease potential in visible light and cellular uptake. The significant results of this study include observation of a wide variation of the visible light-induced photocytotoxic properties of the iron(III) complexes with complex **5** having an increased aromatic surface area being the most active one. The effect of substituent on the photophysical and DNA binding properties of the complexes have been rationalized from the theoretical studies.

EXPERIMENTAL SECTION

Materials and Measurements. The reagents and chemicals were procured from commercial sources (Sigma-Aldrich, U.S.A.; s.d. Fine Chemicals, India) and used as received without any further purification. The solvents used were purified by standard procedures.[22] Supercoiled (SC) pUC19 DNA (cesium chloride purified) was purchased from Bangalore Genei (India). Calf thymus (CT) DNA, bovine serum albumin (BSA), agarose (molecular biology grade), distamycin-A, catalase, superoxide dismutase (SOD), 2,2,6,6-tetramethyl-4-piperidone (TEMP), and ethidium bromide (EB) were from Sigma (U.S.A.). Tris(hydroxymethyl)aminomethane−HCl (Tris−HCl) buffer was prepared using deionized and sonicated triple distilled water. The *N,N*-donor heterocyclic bases, dipyrido-6,7,8,9-tetrahydrophenazine (dpqC),[23] dipyrido[3,2-*a*:2′,3′-*c*]phenazine-11-sulfonic acid (dppzs),[24] dipyrido[3,2-*a*:2′,3′-*c*]phenazine-2-carboxylic acid (dppzc),[25] benzo[*i*]dipyrido[3,2-*a*:2′,3′-*c*]phenazine (dppn),[26] and 7-aminodipyrido[3,2-*a*:2′,3′-*c*]phenazine (dppza)[27] were prepared by following literature procedures. The ligand H_3L was prepared using a literature method that was modified by doing a one-pot Mannich reaction of glycine with 2 equiv of 2,6-di-*tert*-butylphenol in the presence of 2 equiv of paraformaldehyde in an acetic acid medium.[28] The preparative procedure for [FeL(dppz)] (**6**) and [FeL(dpq)], where dppz and dpq are dipyrido[3,2-*a*:2′,3′-*c*]phenazine and dipyrido[3,2-*d*:2′,3′-*f*]quinoxaline, was reported earlier.[21]

The elemental analysis was done using a Thermo Finnigan FLASH EA 1112 CHNS analyzer. The infrared and electronic spectra were recorded on Bruker Alpha FT-IR and PerkinElmer Lambda 650 spectrophotometers, respectively. Magnetic susceptibility data at 298 K for the powdered samples of the complexes were obtained using Model 300 Lewis-coil-force magnetometer (George Associates Inc., Berkeley, U.S.A.) with $Hg[Co(NCS)_4]$ as a standard. Experimental susceptibility data were corrected for diamagnetic contributions.[29] Molar conductivity measurements were done using a Control Dynamics (India) conductivity meter. Cyclic voltammetric measurements were made at 25 °C using EG&G PAR 253 VersaStat potentiostat/galvanostat with a three-electrode configuration consisting of a glassy carbon working, a platinum wire auxiliary, and a saturated calomel reference (SCE) electrode. Ferrocene (E_f = 0.42 V) was used as a standard in MeCN-0.1 M $[Bu^n_4N](ClO_4)$ (TBAP). Electrospray ionization mass and ^1H NMR spectral measurements were made using Esquire 300 Plus ESI Model (Bruker Daltonics) and Bruker 400 MHz NMR spectrometers, respectively. Inductively Coupled Plasma Optical Emission spectral

measurements were carried out using Perkin-Elmer ICP-OES (Model Optima 2000 DV).

Synthesis of [FeL(B)] (B = dpqC, 1; dppzc, 2; dppzs, 3; dppza, 4; dppn, 5). The complexes were prepared by a general preparative procedure in which the ligand H_3L (0.127 g, 0.25 mmol) taken in a mixture of MeOH, EtOH and MeCN (3:3:2 v/v, 20 mL) was reacted with Et_3N (0.1 mL, 0.75 mmol) followed by addition of $Fe(NO_3)_3 \cdot 9H_2O$ (0.102 g, 0.25 mmol). The solution was stirred for 15 min followed by addition of the diimine base (B = 0.072 g, dpqC; 0.082 g, dppzc; 0.091 g, dppzs; 0.074 g, dppza; 0.083 g, dppn). The solution was filtered after 10 min. The filtrate upon slow evaporation gave dark purple microcrystalline solid in an analytically pure form.

*[FeL(dpqC)] (**1**).* Yield, 78% (0.166 g). Anal. Calcd for $C_{50}H_{60}FeN_5O_4$: C 70.58; H, 7.11; N, 8.23. Found: C, 70.44; H, 7.21; N 8.18. Molar conductance in DMF (Λ_M): 17 S m^2 M^{-1}. FT-IR (KBr phase): 2952vs, 1663vs (ν_{COO}), 1515s, 1468 m, 1356s, 1304 m, 1237s, 1168s, 1107w, 919 m, 876w, 731s, 637w, 608w, 540 m, 475 m cm^{-1} (vs, very strong; s, strong; m, medium; w, weak). ESI-MS in MeCN (m/z): 851.3 $(M+H)^+$. UV−visible in 6% DMF/Tris HCl buffer [λ_{max}, nm (ε, M^{-1} cm^{-1})]: 485 (5380), 348 (22,790), 332 (24,080), 285 (41,500), 260 (66,200). μ_{eff} (298 K): 5.89 μ_B [χ_M (corrected) = 0.01454 cm^3 M^{-1}].

*[FeL(dppzc)] (**2**).* Yield, 54% (0.121 g). Anal. Calcd for $C_{51}H_{56}FeN_5O_6$: C, 68.76; H, 6.34; N, 7.86. Found: C, 68.55; H, 6.43; N, 7.71. Λ_M in DMF: 17 S m^2 M^{-1}. FT-IR (KBr phase): 2952vs, 1663vs (ν_{COO}), 1515s, 1468 m, 1356s, 1304 m, 1267 m, 1237s, 1169 m, 1128 m, 1076 m, 942w, 912 m, 876w, 835 m, 737s, 609 m, 543s, 485 m, 405 m cm^{-1}. ESI-MS in MeCN (m/z): 892.3 $(M+H)^+$. UV−visible in 6% DMF/Tris-HCl buffer [λ_{max}, nm (ε, M^{-1} cm^{-1})]: 475 (5200), 385 (18,920), 368 (18,800), 295 (39,900), 276 (66,200). μ_{eff} (298 K): 5.83 μ_B [χ_M (corrected) = 0.01424 cm^3 M^{-1}].

*[FeL(dppzs)] (**3**).* Yield, 57% (0.132 g). Anal. Calcd for $C_{50}H_{56}FeN_5O_7S$: C, 64.79; H, 6.09; N, 7.56; S, 3.46. Found: C, 64.68; H, 6.18; N, 7.66; S, 3.39. Λ_M in DMF: 30 S m^2 M^{-1}. FT-IR (KBr phase): 2954s, 1669s (ν_{COO}), 1474 m, 1444w, 1356vs, 1332vs, 1243 m, 1203w, 1089w, 1075 m, 1029s, 929w, 875w, 834 m, 736 m, 678 m, 599 m, 546w, 477w cm^{-1}. ESI-MS in MeCN (m/z): 927.3 $(M+H)^+$. UV−visible in 6% DMF/Tris HCl buffer [λ_{max}, nm (ε, M^{-1} cm^{-1})]: 495 (5,250), 380 (15,440), 362 (16,120), 344 (14,440), 271 (57,800). μ_{eff} (298 K): 5.89 μ_B [χ_M (corrected) = 0.01454 cm^3 M^{-1}].

*[FeL(dppza)] (**4**).* Yield, 85% (0.183 g). Anal. Calcd for $C_{50}H_{57}FeN_6O_4$: C, 69.68; H, 6.67; N, 9.75. Found: C, 69.44; H, 6.71; N, 9.72. Λ_M in DMF: 21 S m^2 M^{-1}. FT-IR (KBr phase): 3498 w, 3322w, 3196w, 2951 m, 1666vs (ν_{COO}), 1532w, 1504 m, 1463 m, 1431 m, 1412 m, 1359s, 1314 m, 1237s, 1198 m, 1079s, 917w, 876 m, 854 m, 827s, 736s, 665 m, 607w, 539 m, 474 m cm^{-1}. ESI-MS in MeCN (m/z): 862.3 $(M+H)^+$. UV−visible in 6% DMF/Tris HCl buffer [λ_{max}, nm (ε, M^{-1} cm^{-1})]: 455 (12,650), 307 (36,390), 278 (44,840). μ_{eff} (298 K): 5.91 μ_B [χ_M (corrected) = 0.01463 cm^3 M^{-1}].

*[FeL(dppn)] (**5**).* Yield, 69% (0.154 g). Anal. Calcd for $C_{54}H_{58}FeN_5O_4$: C, 72.31; H, 6.52; N, 7.81. Found: C, 72.14; H, 6.58; N, 7.73. Λ_M in DMF: 15 S m^2 M^{-1}. FT-IR (KBr phase): 2954vs, 1665vs (ν_{COO}), 1469 m, 1360s, 1300 m, 1241s, 1168s, 920w, 877 m, 838 m, 744s, 611 m, 616w, 557 m, 484 m cm^{-1}. ESI-MS in MeCN (m/z): 898.4 $(M+H)^+$. UV−visible in 6% DMF/Tris HCl buffer [λ_{max}, nm (ε, M^{-1} cm^{-1})]: 480 (10,760), 416 (13,570), 394 (14,750), 314 (41,400), 278 (49,560). μ_{eff} (298 K): 5.88 μ_B [χ_M (corrected) = 0.01449 cm^3 M^{-1}].

The complexes were soluble in CH_2Cl_2, MeOH, EtOH, MeCN, DMF, and DMSO. The solution stability of the complexes was adjudged from the presence of an essentially single mass peak pertaining to the protonated molecular ion $[M+H]^+$ in the ESI-MS spectra of the complexes (Supporting Information, Figures S1−S5).

DNA and Protein Binding Experiments. The DNA binding experiments were done in Tris-HCl/NaCl buffer (5 mM Tris-HCl, 5 mM NaCl, pH 7.2) or phosphate buffer pH 7.4 using DMF solution of the complexes **1**−**5** using procedures as reported earlier (see Supporting Information for details).[30−35] The protein binding experiments were carried out with 2 μM BSA in phosphate buffer (pH 7.2) by fluorescence spectroscopy.[36]

DNA Photocleavage Experiments. DNA photocleavage studies were carried out using DMF solutions of the complexes **1**−**5** and supercoiled pUC19 DNA in 50 mM Tris HCl buffer containing 50 mM NaCl at 476, 530, and 647 nm wavelengths (Spectra Physics Water-Cooled Mixed-Gas Ion Laser Stabilite 2018-RM having continuous-wave (CW) beam diameter $1/e^2$ 1.8 mm ±10% and beam divergence with full angle 0.7 mrad ±10%, laser power 50 mW measured using Spectra Physics CW Laser Power Meter Model 407A) using appropriate controls and inhibitors as described previously (see Supporting Information for details).[37]

Cell Cytotoxicity Assay. Photocytotoxicity of the iron(III) complexes were assessed using 3-(4,5-dimethyl-2-thiazolyl)-2,5-diphenyl-2*H*-tetrazolium bromide (MTT) assay based on the ability of mitochondrial dehydrogenases in the viable cells to cleave the tetrazolium rings of MTT forming dark blue membrane impermeable crystals of formazan that can be quantified at 595 nm on detergent solubilization.[38] The quantity of the formazan product formed gave a measure of the number of viable cells. Approximately, 8000 cells of human cervical carcinoma (HeLa) were plated in 96 wells culture plate in DMEM containing either 10% FBS and after 24 h of incubation at 37 °C in CO_2 incubator, different concentrations of the iron complexes or cisplatin dissolved in 1% DMSO were added to the cells and incubation was continued for 4 h in dark, followed by exposure to 400−700 nm visible light from a Luzchem Photoreactor (light dose: 10 *J* cm^{-2}). Post irradiation, PBS was replaced with DMEM-FBS and incubation was continued for a further period of 12 h in dark. After the incubation period, a 20 μL of 5 mg mL^{-1} of MTT was added to each well and incubated for an additional period of 3 h. The culture medium was discarded and 100 μL of 10% SDS/0.01 N HCl was added to dissolve the purple formazan crystals, and the absorbance at 595 nm was noted using a BIORAD ELISA plate reader. Cytotoxicity of the complexes was measured as the percentage ratio of the absorbance of the treated cells to the untreated controls. The dppz complex **6** was used as a control. The IC_{50} values were determined by nonlinear regression analysis (GraphPad Prism 5.1).

Cellular Uptake Measurements. For cellular uptake studies, HeLa cells were grown until 80% confluency in 90 mm^2 cell culture flasks in DMEM medium supplemented with 10% FBS.[39] The complexes **1**−**5**, [FeL(dpq)] and [FeL(dppz)] (**6**) dissolved in DMSO were then added to the cells to give complex concentration of 25 μM (final DMSO concentration of 1% v/v). The cells were then incubated for 4 h at 37 °C in a CO_2 incubator. At the end of the incubation period, the culture medium was discarded, and the cells were washed thrice with ice cold PBS (pH 7.4). The cells were then harvested, taken up in PBS followed by centrifugation for 10 min at 3000 rpm and 4 °C. The resulting pellet, after discarding PBS, was dissolved in 70% nitric acid at 65 °C for 2 h. The samples were diluted to final 5% nitric acid concentration with double distilled water containing 0.1% Triton X. The iron content of the samples was determined using inductively coupled plasma-optical emission spectrometry (ICP-OES) at the emission wavelengths of 238.204 and 239.562 nm for iron. The protein content was estimated after lysing the cell pellet (obtained by similar treatment of HeLa cells with the complexes followed by isolation by scraping) with 1 N NaOH. The total iron content of the samples is expressed as the quantity of iron in ng per mg protein.

Nuclear Staining. 4′,6-Diamidino-2-phenylindole (DAPI) staining was carried out to monitor the changes in nuclear morphology and chromatin organization following photoexposure after treatment with the dppn complex **5**.[40] Briefly, the control and the cells were treated with complex **5** (10 μM) for 4 h in dark followed by irradiation with visible

light of 400−700 nm (10 $J\ cm^{-2}$). After 2 h incubation in fresh media the samples were fixed with 3.7% (v/v) paraformaldehyde in PBS for 10 min at room temperature, and then stained with DAPI (10 $\mu g\ mL^{-1}$ in PBS) for 5 min. The cells after being washed thrice with PBS were examined under a fluorescence microscope with 360/40 nm excitation and 460/50 nm emission filters. The live cells were identified by essentially no or very low nuclear staining and the cell morphology. The apoptotic cells that uptake DAPI were identified by the presence of highly condensed or fragmented nuclei with significant alteration in cell morphology.

Computational Study. The geometries of all iron(III) complexes were optimized by using the Gaussian03 and Gaussian09 suite of programs,[41] with the hybrid HF-DFT method B3LYP.[42] A def2-TZVP basis set ("triple-ζ valence" plus polarization functions) was used for iron atom and 6-311G basis set was used for C, H, N, O, and S atoms in all the calculations.[43] Time-dependent density functional theory (TD-DFT) calculations were carried out to investigate the optical properties of the complexes. The lowest 40 transitions, up to 400 nm, were taken into account in the calculations of the absorption spectra. We also made use of the natural bond orbital (NBO) theory to determine the nature of the molecular orbitals.[44]

Molecular docking calculations were done using the Gold Suite which is based on genetic algorithm.[45] The CHARMm force-field was used for the metal complex in the input of the calculations. Because of the higher hybridization state of the iron atom in the complex, due correction of the partial charge distribution for all atoms in the ligand was made following the output from Gaussian03. Energy-minimized structures of complexes **1**−**5** were generated from the coordinates of the crystal structure of complex **6**. The structure of the B-DNA sequence $d(GACATGTC)_2$ (PDB code 202D) was downloaded from the protein data bank (PDB). The water molecules and the ligand menogaril were removed before performing docking calculations. The binding site was assigned across the minor and major grooves of the DNA molecule. The docking was performed to find the most stable and favorable orientation. The docking parameters for the calculation were carried out with an initial population of 100 and 5×10^5 energy evaluations. The mutation frequency and crossover frequency were 95.

RESULTS AND DISCUSSION

Synthesis and General Properties. The iron(III) complexes [FeL(B)] (**1**−**5**) were synthesized in good yields from the reaction of $Fe(NO_3)_3 \cdot 9H_2O$ with H_3L and the modified dipyridophenazine bases (B: dpqC, **1**; dppzc, **2**; dppzs, **3**; dppza, **4**; dppn, **5**) (Chart 1). Our objective in designing [FeL(B)] species is to have a bioessential redox active metal center like iron(III) to facilitate photoredox DNA cleavage pathway, the trianionic tetradentate ligand H_3L with two phenolates, one amine and one acetate O-donor site to ensure stability of the iron(III) redox state in a reducing environment which exists inside the cells, and dipyridophenazine-based ligands having photoactive phenazine moieties. Besides having the basic requirements for PDT, the use of *tert*-butyl groups in L is likely to enhance the cellular uptake as has been found in case of lipophilic drugs.[46] Again, the choice of iron(III)-phenolates is based on the fact that such a moiety is well-known to show broad low energy charge-transfer transitions which is important for PDT drug designing.[47] The photosensitizing property has been suitably incorporated into the complexes with bidentate dipyridophenazine-based photoactive ligands having phenazine moiety that are present in antitumor antibiotics like echinomycin or triostin and are known to generate photoexcited $^3(n-\pi^*)$ or $^3(\pi-\pi^*)$ state cleaving DNA on photoirradiation with UV light.[48,21] The use of modified dppz ligands is to study the structure−activity relationship of the complexes. The complexes have been characterized from analytical and spectral studies (Table 1). The crystal structure of the dppz complex which is used as a control species has been reported by us.[21]

All the complexes are discrete monomeric and nonelectrolytic in solution. They do not have any labile ligands as evidenced from the mass spectral studies in MeCN showing essentially the molecular ion peak. The electronic spectra of the complexes show a broad band near 500 nm with an absorption tail that extends to the PDT spectral window in 6% DMF/5 mM Tris HCl buffer (Figure 1, Supporting Information, Figures S6−S9). This spectral feature has enabled us to use red light laser for DNA photocleavage studies. Use of red light in PDT is important considering deeper skin penetration of red light.[49] The visible spectral band is assignable to the phenolate-to-iron(III) charge transfer.[21] Complexes **4** and **5** with respective dppza and dppn as the photosensitizer ligand display an additional absorption band near 450 nm. Magnetic susceptibility measurements on the solid powdered samples of the complexes at 25 °C gave a magnetic moment value of ∼5.9 μ_B corresponding to five unpaired electrons indicating high-spin nature of the $3d^5$-iron(III) complexes. Cyclic voltammetric studies revealed that the complexes are redox-active showing Fe(III)/Fe(II) couple near −0.7 V (vs SCE) in DMF-0.1 M TBAP. Complexes **1** and **2** showed the presence of only a cathodic response at −0.64 and −0.77 V without having any anodic counterpart, whereas complexes **3**−**5** displayed quasi-reversible cyclic voltammetric response near −0.7 V versus SCE (Table 1, Figure 1, Supporting Information, Figures S10−S13). The redox potential of about −0.7 V indicates stability of the ferric state over the reduced ferrous state in these complexes. Complex **2** displayed an irreversible cyclic voltammetric response at −1.32 V assignable to the dppzc reduction. Complex **4** showed irreversible cyclic voltammetric responses at −0.99, −1.16, and −1.4 V assignable to the dppza reduction. Complex **5** displayed a quasi-reversible voltammogram at −0.92 V versus SCE (ΔE_p = 80 mV) because of dppn reduction. The reversibility of the process could be due to the presence of extended aromatic moiety in the dppn ligand.

DNA and Protein Binding. The DNA binding propensity of the ternary iron(III) complexes was studied by various spectral techniques using calf-thymus (CT) DNA (Table 1). The equilibrium binding constant (K_b) values were obtained from the absorption spectral titration of the complexes with CT-DNA (Supporting Information, Figures S14−S18). The spectral bands that were monitored to determine the K_b values were 259, 271, 275, 278, and 279 nm for the complexes **1**−**5**, respectively. The bathochromic shifts associated with these spectral bands ranged between 0 and 3 nm which might be a consequence of groove binding preference of these complexes. Complex **5** with an extended planar moiety in the dppn ligand showed the highest DNA binding propensity with a K_b value of $2.66 \times 10^6\ M^{-1}$ because of the ability of the dppn ligand to undergo strong π-stacking interactions with the purine and pyrimidine DNA bases. The binding strength of the dppn complex **5** is significantly higher than [FeL(dppz)] (**6**) which has a binding constant value of $3.2 \times 10^5\ M^{-1}$ with CT-DNA.[21] Complex **4** with an amine group on the dppz ring showed considerably higher binding propensity as compared to its parent complex **6**. This could be due to additional hydrogen bonding ability of complex **4** imparted by the amine group. Complexes **2** and **3** having dppzc and dppzs respectively displayed lesser DNA binding propensity

Table 1. Selected Physicochemical Data[a] for the Complexes 1−6

	[FeL(dpqC)] (**1**)	[FeL(dppzc)] (**2**)	[FeL(dppzs)] (**3**)	[FeL(dppza)] (**4**)	[FeL(dppn)] (**5**)	[FeL(dppz)] (**6**)
IR[b] /cm^{-1} ν (C=O)	1663	1669	1661	1666	1665	1667
λ, nm (ε, M^{-1} cm^{-1})[c]	485 (5,380)	475 (5,200)	495 (5,245)	455 (12,650)	480 (10,460)	475 (5,340)
E_f[d]/ V (ΔE_p,mV)	−0.64[e]	−0.77[e]	−0.68 (90)	−0.69 (113)	−0.67 (110)	−0.61 (98)
ΔT_m[f]/ °C	2.6	2.2	1.5	4.1	5.0	3.0
K_b/ M^{-1} [s/ b.p.][g]	2.2(±0.4) × 10^5 [0.5]	2.9(±0.8) × 10^5 [0.14]	1.4(±0.3) × 10^5 [0.24]	6.6 (±1.4) × 10^5 [0.1]	2.6(±0.6) × 10^6 [0.6]	3.2(±0.9) × 10^5 [0.4]
K_{app}[h]/ M^{-1}	3.1 × 10^5	4.5 × 10^5	1.5 × 10^5	6.8 × 10^5	3.0 × 10^6	5.7 × 10^5
K_{BSA}[i]/M^{-1}	1.6 × 10^5	6.2 × 10^5	3.4 × 10^5	2.3 × 10^5	2.0 × 10^5	1.1 × 10^5

[a] Data for complex **6** are from ref 21. [b] In KBr phase. [c] Visible electronic band in 6% DMF-Tris-HCl buffer. [d] Scan rate of 50 mV s^{-1} in DMF-0.1 M TBAP. Potentials are vs saturated calomel electrode (SCE). $E_f = 0.5(E_{pa} + E_{pc})$. $\Delta E_p = (E_{pa} - E_{pc})$, where E_{pa} and E_{pc} are anodic and cathodic peak potentials, respectively. [e] Cathodic peak potential. [f] Change in the DNA melting temperature. [g] K_b, DNA binding constant (s, MvH equation fitting parameter). [h] K_{app}, apparent DNA binding constant. [i] K_{BSA}, Stern−Volmer quenching constant for BSA fluorescence.

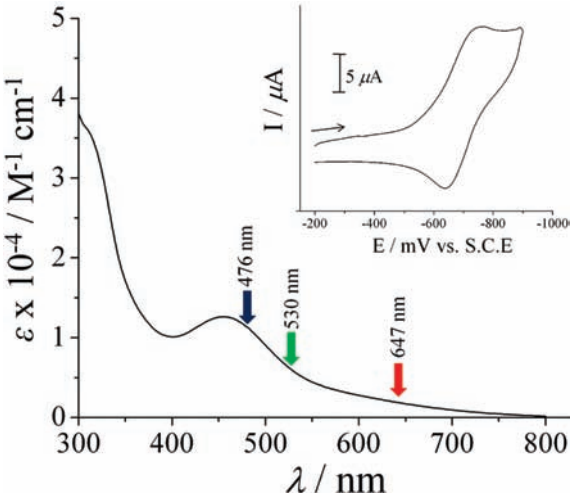

Figure 1. Electronic absorption spectrum of complex **4** in 6% DMF-Tris HCl buffer with arrows showing selected wavelengths used for DNA photocleavage studies. The inset shows the cyclic voltammogram of complex **4** in DMF-0.1 M TBAP at a scan rate of 50 mV s^{-1}.

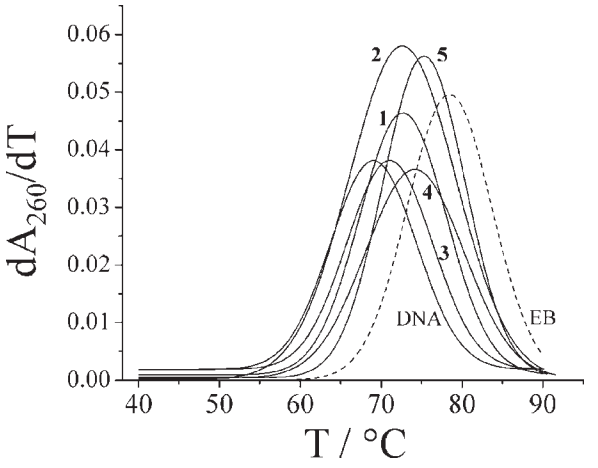

Figure 2. Derivative plots (dA_{260}/dT vs T) of the thermal denaturation of 150 μM NP CT DNA between 40 and 90 °C measured at 260 nm in absence and in the presence of 10 μM of **1**−**5** and ethidium bromide. The dashed line shows the derivative plot for thermal denaturation of CT-DNA in presence of ethidium bromide (EB, 10 μM).

than that of complex **6** (Table 1). The lower binding constant for these two complexes compared to **4** and **6** may be attributed to the steric effects arising out of the substituents of the dppz ring. Moreover, a comparison between the K_b values of **2** and **3** indicate that complex **2** binds more efficiently to CT-DNA than complex **3**, which may be ascribed to the hydrogen bonding ability of the carboxylate group with the DNA bases. Moreover, the sulfonic acid group is nonplanar unlike the carboxylate group and because of its higher van der Waals radii sterically inhibits insertion of the phenazine ring into the DNA base pairs. Complex **1** containing dpqC ligand showed nearly similar DNA binding strength as that of its analogue [FeL(dpq)] but lesser than that of complex **6**.[21] This observation indicates that the presence of a nonplanar cyclohexyl ring in dpqC does not augment the binding propensity of complex **1**. The results obtained here points to the fact that the presence of planar aromatic rings is therefore of paramount importance for intercalative DNA binding interactions as observed in the UV−visible titration experiments with CT-DNA. The DNA binding strength of the complexes follows the order: **5** (dppn) > **4** (dppza) > **6** (dppz) > **1** (dpqC) > **2** (dppzc) > **3** (dppzs).

Competitive ethidium bromide displacement assay was carried out to further confirm the observed DNA binding trend of the iron(III) complexes as observed in the UV−visible titration experiments (Supporting Information, Figure S19). This assay is based on the quenching of ethidium bromide fluorescence upon displacement of the DNA-bound ethidium bromide by the complexes. The quenching of ethidium bromide fluorescence occurs because of proton transfer from its singlet excited state to water.[50] The apparent binding constant (K_{app}) value gives an estimate of the binding of the complexes to DNA relative to ethidium bromide, the well-known DNA intercalator. The results obtained show that the DNA binding affinity of the complexes follows the order: **5** > **4** > **1** > **2** > **3** which is in excellent agreement with the DNA binding order obtained from absorption titration experiments (Table 1). Thermal denaturation experiments were carried out to monitor the changes in the double helical structure upon complex binding. An increase in melting temperature (T_m) pertains to stabilization of the DNA double helical structure whereas a decrease signifies its destabilization upon complex binding. Moreover, the extent of change in melting temperature can also be related to groove and/or intercalative modes of binding of the complexes to CT DNA.[51] The change in melting temperatures observed for the complexes **1**− **6** ranged between 1.4 to 5 °C indicating partial intercalative mode of interaction of the complexes to DNA (Figure 2). The melting data suggest that the presence of sterically demanding *tert*-butyl groups on the tetradentate ligand prevents complete

dx.doi.org/10.1021/ic1024229 |*Inorg. Chem.* 2011, 50, 2975–2987

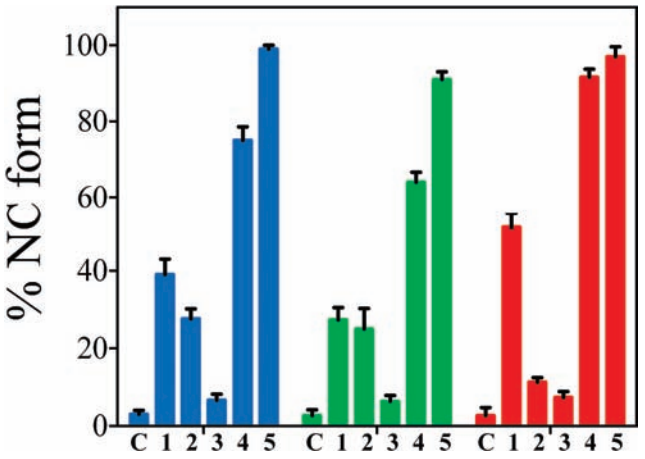

Figure 3. Bar diagram shows the extent of DNA photocleavage induced by the complexes **1**−**5** in 10% DMF/50 mM Tris HCl buffer. The blue, green, and red bars correspond to 476, 530, and 647 nm wavelengths, respectively. C stands for DNA control. The numbers **1**−**5** in the *x*-axis correspond to the complex numbers **1** to **5**.

intercalation of the extended planar rings of the phenazine bases present in the complexes into the DNA. The dppn complex showed better DNA intercalative binding mode than other complexes.

Since serum albumin constitutes ∼55% of the total protein in blood plasma and it plays a pivotal role in drug transport and drug metabolism, the interaction of the iron(III) complexes with serum albumin was studied from the binding experiments with BSA as a model protein using tryptophan fluorescence quenching assay.[52] The intrinsic fluorescence of BSA arises owing to the presence of two tryptophan residues at positions 134 and 212 in a hydrophobic environment. The fluorescence intensity is thus dependent on their exposure to the surrounding polar environment. The binding of small molecules to BSA is associated with detectable changes in the fluorescence intensity because of changes in the surrounding environment around the tryptophan residues. The fluorescence intensity of BSA has been found to decrease with gradual increase in the concentration of the complexes **1**−**5** (Supporting Information, Figure S20). This decrease in fluorescence intensity possibly arises because of perturbations in the secondary structure of BSA leading to the exposure of the tryptophan residues to the immediate polar environment. The hydrophobic *tert*-butyl groups present in the complexes might also be playing a crucial role in hydrophobic interactions with BSA, a well-known transporter of hydrophobic molecules. Complex **2** showed the highest BSA binding propensity among all the complexes possibly because of the hydrogen bonding ability of the carboxylate group with the peptide backbone (Table 1). This K_{BSA} value is also higher than that of complex **6** and [FeL(dpq)].[21] The results indicate that the complexes bind favorably to serum protein which could further enhance its half-life inside the body and transport to its target tissues.

DNA Photocleavage. To ascertain the DNA photocleavage potential of the iron(III) complexes, studies were carried out using SC pUC19 DNA (33.3 μM, 0.2 μg) in Tris-HCl/NaCl (50 mM, pH, 7.2) buffer on irradiation with visible light of wavelengths 476, 530, and 647 nm (50 mW) using a CW Argon−Krypton mixed gas ion laser. The agarose gel electrophoresis diagram showing the extent of DNA cleavage from SC to the nicked circular (NC) form is shown in Figure 3 and selected DNA photocleavage data are given in Table 2 (Supporting Information, Figures S21−S23). Control experiments with the salt $Fe(NO_3)_2 \cdot 9H_2O$ (30 μM) and the ligands (30 μM) alone did not show any significant photocleavage of DNA at these visible wavelengths, although the dppn ligand displays moderate photocleavage activity (∼20% NC form). DNA samples treated with the complexes **1**−**5** but unexposed to light were also ineffective in causing any DNA cleavage. Moreover, the use of various wavelengths to test the photonuclease activity is justified since the complexes possess a broad absorption tail which extends into the PDT spectral window of 620−850 nm. Complex **5** with dppn as the photosensitizer showed remarkable photonuclease potential among the complexes studied. A 30 μM solution of complex **5** essentially completely cleaved SC-DNA to its NC form at 476 nm in 30 min photoexposure (Figure 3). This possibly results from the high DNA binding affinity of the dppn complex **5** and also because the dppn ligand possesses two absorption bands at lower energy than the other modified dipyridophenazine bases used in this study. Complex **4** also acts as an efficient photonuclease with complete cleavage of SC DNA to NC form with 30 μM concentration in 1 h photoexposure at 476 nm. Complex **3**, with dppzs as the photosensitizer, showed the lowest photonuclease ability, which might be a consequence of its comparatively low binding ability to DNA. The dpqC complex **1** showed good DNA photocleavage activity at a concentration of 30 μM, and the cleavage activity is comparable to the photonuclease potential of [FeL(dpq)] and complex **6**.[21] The dppzc complex **2** showed moderate photonuclease potential at the studied wavelengths, but is less effective than complex **1**. The complexes exhibited significant activity in green light of 530 nm and red light of 647 nm. Complexes **4** and **5** completely cleaved SC DNA to its NC form in red light upon irradiation for 2 h. Photocleavage of SC DNA in red light by **2** and **3** was insignificant. Complex **1** photocleaved SC DNA to ∼51% NC form under similar conditions. Together, the results indicate that substitution on the phenazine ring with electron-withdrawing substituents reduces the photonuclease ability of the complexes. The extent of DNA photocleavage follows the spectral pattern as the extinction coefficient of the iron(III)-phenolate charge-transfer band decreases with increasing wavelength.

The mechanistic aspects of the photoinduced DNA cleavage activity of complex **5** were investigated using various additives (Figure 4). Addition of singlet oxygen quenchers DABCO, TEMP, sodium azide, and L-histidine caused no reduction in the DNA cleavage activity at 476 nm. However, hydroxyl radical scavengers like DMSO and KI significantly reduced the DNA cleavage activity. Catalase and SOD, which are respective hydrogen peroxide and superoxide scavengers, also showed inhibition in the DNA photocleavage activity. The results suggest the involvement of hydroxyl radicals ($HO^{\bullet}$) and superoxide radicals ($O_2^{\bullet -}$) in the photocleavage reaction in visible light. The involvement of singlet oxygen in the photonuclease activity was further excluded by the fact that no significant enhancement in DNA cleavage was observed in presence of D_2O, which is known to enhance the lifetime of singlet oxygen.[53] We have studied the groove binding preference of the complexes using distamycin-A and methyl green as DNA minor and major groove binders. They alone showed ∼6% and ∼19% cleavage

Table 2. Selected DNA Photocleavage Data of the Iron(III) Complexes 1−6

complex	% NC form (476 nm[a])	% NC form (530 nm[a])	% NC form (647 nm[b])
DNA control	2	2	3
[FeL(dpqC)] (**1**)	39	31	51
[FeL(dppzc)] (**2**)	28	25	12
[FeL(dppzs)] (**3**)	7	5	9
[FeL(dppza)] (**4**)	74	65	94
[FeL(dppn)] (**5**)[c]	98	99	98
[FeL(dppz)] (**6**)[d]	48	37	68

[a] The photoirradiation time was 30 min with 50 mW Ar−Kr laser power. [b] The photoirradiation time was 2 h with 50 mW Ar−Kr laser power. [c] DNA treated with complex **5** but unexposed to light showed about 5% NC form. [d] Data from ref 21.

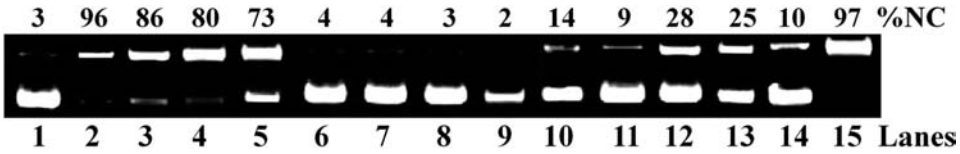

Figure 4. Mechanistic aspects of the photocleavage of SC pUC19 DNA (0.2 μg, 30 μM) by complex **5** (30 μM) in 50 mM Tris-HCl/NaCl buffer (pH, 7.2) containing 10% DMF on photoirradiation at 476 nm (50 mW) for 30 min in the presence of different additives: lane 1, DNA control; lane 2, DNA + **5**; lane 3, DNA + TEMP (500 μM) + **5**; lane 4, DNA + DABCO (500 μM) + **5**; lane 5, DNA + NaN_3 (500 μM) + **5**; lane 6, DNA + KI (500 μM) + **5**; lane 7, DNA + DMSO (4 μL) + **5**; lane 8, DNA + catalase (4 units) + **5**; lane 9, DNA + SOD (4 units) + **5**; lane 10, DNA + mannitol (500 μM) + **5**; lane 11, DNA + **5** (argon, 2 h); lane 12, DNA + methyl green (50 μM) + **5**; lane 13, DNA + methyl green (50 μM); lane 14, DNA + distamycin (50 μM); lane 15, DNA + distamycin (50 μM) + **5**.

Table 3. Photocytotoxicity of the Iron(III) Complexes

	IC_{50} value (in μM) in HeLa	
complex	dark	visible light (400−700 nm, 10 J cm^{-2})
[FeL(dpq)][a]	>100	>100
[FeL(dpqC)] (**1**)	>150	35.5 ± 2.4
[FeL(dppzc)] (**2**)	>150	61.1 ± 1.6
[FeL(dppzs)] (**3**)	>150	73.4 ± 2.7
[FeL(dppza)] (**4**)	>150	5.3 ± 1.4
[FeL(dppn)] (**5**)	>100	0.77 ± 0.13
[FeL(dppz)] (**6**)	>100	7.5 ± 1.6 [3.59 ± 1.2][a,b]
cisplatin	71.3 ± 2.9	68.7 ± 3.4
photofrin	>41[c]	4.28 ± 0.2[c]

[a] The values are from ref 21. [b] This value corresponds to visible light (400−700 nm) treatment with light dose of 20 J cm^{-2} (ref 21). [c] This IC_{50} value is taken from ref 2 and converted from μg mL^{-1} to μM using the average molecular weight of Photofrin as 600 g M^{-1}.

respectively of the SC DNA at 476 nm for an exposure time of 0.5 h. Addition of **1** or **5** (10 μM) to distamycin-A bound DNA showed no reduction in photonuclease activity of the complex, whereas a similar study with methyl green bound DNA showed inhibition of photonuclease activity for both suggesting major groove-binding propensity of these complexes (lanes 12−15 in Figure 4).[54] The necessity of molecular oxygen in the DNA photocleavage activity of the iron(III) complexes was proved by carrying out the reaction in an argon atmosphere where no significant photocleavage was observed. Taken together, visible light mechanistic data point to a photoredox pathway whereby metal reduction following photoactivation of the LMCT band might result in a charge separated $Fe^{2+}-L^{\bullet+}$ (phenolate ligand radical cation) as the reactive species that possibly reduces O_2 to $O_2^{\bullet-}$ by the reactive Fe^{2+} ion with subsequent formation of hydroxyl radicals in the reaction: $3O_2^{\bullet-} + 2H^+ \rightarrow HO^{\bullet} + HO^- + 2O_2$. Such a mechanism is known to be operative for a wide range of iron(III) complexes having phenolate ligands.[55] This DNA photocleavage mechanism is different from that of the iron(III) complex reported by Zaleski and co-workers, which cleaves DNA by generation of dinitrogen radical upon excitation of the ligand-to-metal charge transfer (LMCT) band of the complex.[56]

Cell Cytotoxicity. The photocytotoxic abilities of the iron(III) complexes of modified dipyridophenazine ligands were tested in HeLa cells upon irradiation with broadband light source (400−700 nm, 10 J cm^{-2}), and the cell viability was assessed using MTT assay (Table 3, Figure 5, Supporting Information, Figure S24). Complexes **1**−**5** caused dose-dependent decrease in cell viability. The dppn complex **5** showed >100 fold increase in cytotoxicity upon irradiation with light with an IC_{50} value of 774 nM in light and >150 μM in dark. The dpqC complex **1** although showed a significant improvement in cytotoxicity upon photoexcitation (IC_{50} = 35.5 μM), the results are of interest considering the fact that its analogue [FeL(dpq)] which has a quinoxaline ring did not exhibit any dark or light toxicity (Supporting Information, Figure S24).[21] This could be due to the exposed lone pairs of the nitrogen atoms of the quinoxaline ring in dpq which may reduce its cellular uptake or could be due to faster efflux or faster metabolism in intracellular environment. The dpqC complex **1** possesses a cyclohexane ring which protects the nitrogen atoms thus protecting the exposed lone pairs of nitrogen. Complex **3** with a $-SO_3H$ group on the phenazine moiety gave an IC_{50} value of 73.4 μM in visible light. The photocytotoxic behavior of complex **2** is also not much pronounced as compared to that of the complexes **1**, **4**, and **5**, but it is marginally higher than its sulfonic acid counterpart. This contrasting behavior of the complexes could result from the differences in their lipophilic character as well as trafficking of the molecules to various organelles, thereby affecting the specific organelle where it

dx.doi.org/10.1021/ic1024229 |Inorg. Chem. 2011, 50, 2975–2987

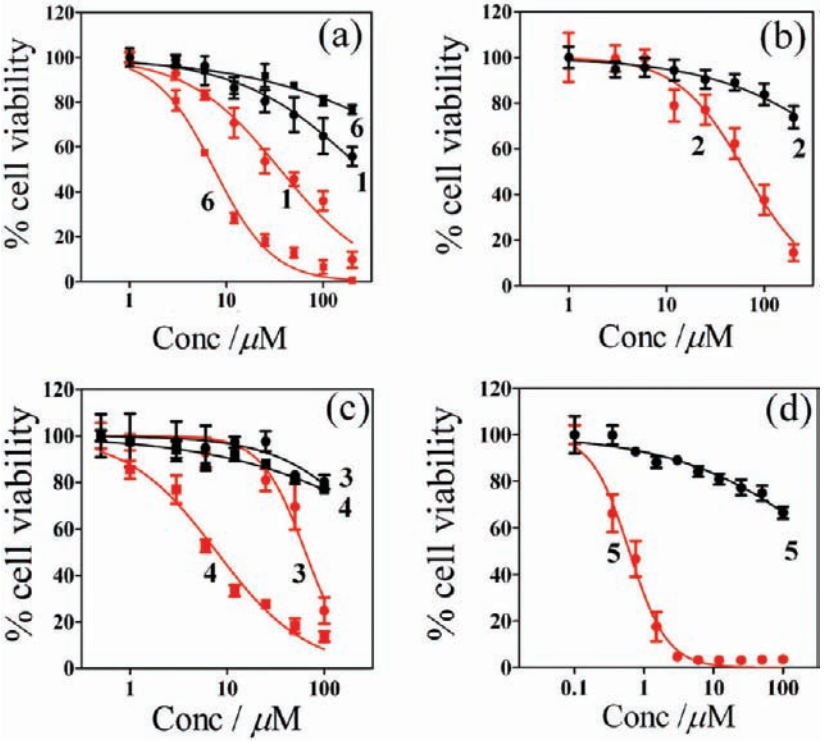

Figure 5. MTT assay to estimate the photocytotoxicity of the iron(III) complexes in HeLa cells: (a) effect of visible light exposure (400−700 nm, 10 $J\ cm^{-2}$) on HeLa cells upon pretreatment with **1** (circle) and **6** (square); (b) visible light exposure (400−700 nm, 10 $J\ cm^{-2}$) on HeLa cells upon pretreatment with **2**; (c) visible light exposure (400−700 nm, 10 $J\ cm^{-2}$) on HeLa cells upon pretreatment with **3** (circle) and **4** (square); and (d) effect of visible light exposure (400−700 nm, 10 $J\ cm^{-2}$) on HeLa cells upon pretreatment with **5**. The dark symbols denote cells treated with the complexes but unexposed to light whereas the red symbols denote cells treated with the complexes and exposed to visible light.

Table 4. Cellular Uptake (ng Fe/mg protein) in HeLa Cells for Incubation with 25 μM of the Complexes [FeL(B)][a] for 4 h

complex	diimine ligand (B)	HeLa
untreated control[b]	N.A.	3.402
[FeL(dpqC)] (**1**)	dpqC	3.883
[FeL(dppzc)] (**2**)	dppzc	3.664
[FeL(dppzs)] (**3**)	dppzs	4.822
[FeL(dppza)] (**4**)	dppza	4.311
[FeL(dppn)] (**5**)	dppn	3.826
[FeL(dppz)] (**6**)	dppz	3.762

[a] The iron(III) concentration in HeLa treated with 25 μM of [FeL(dpq)] was found to be 3.811 ng/mg protein. [b] Cellular iron content in untreated cells.

accumulates. The SO_3H derivatives of rhenium polypyridyl complexes have been found to localize in digestive vacuoles, and the CO_2H derivatives of ruthenium complexes localize more or less to the nucleus, whereas the ruthenium complexes of dppn ligand have been found to damage DNA and nucleoproteins.[57,58] Complex **4** showed good photocytotoxicity with an IC_{50} value of 5.3 μM and negligible dark toxicity. This clearly demonstrates that substitution has significant effect on the photocytotoxic ability and trafficking of these iron(III) complexes. The presence of triglyceride rich plasma membrane in cancer cells probably plays a crucial role in the uptake of this lipophilic molecule.[59]

Cellular Uptake. To test whether increase or decrease in lipophilicity of the photosensitive dipyridophenazine core has any predominant effect on the uptake of these molecules into HeLa cells, we estimated the total iron present in the cell lysates 4 h after incubation with the complexes **1**−**6** in dark and also with [FeL(dpq)] using ICP-OES analysis (Table 4). The cellular uptake profile showed an unexpected trend in uptake of these molecules. Cells treated with complex **3** showed the highest iron content compared to the other members of the series followed by complex **4**. Complexes **1**, **2**, **5**, **6**, and [FeL(dpq)] were found to be uptaken by the HeLa cells almost to a similar extent. The rationale behind this could be the enhanced water solubility imparted by the sulfonic acid group present in complex **3**. Complex **4** because of the presence of terminal amine group is more soluble in aqueous solvents. However, the low photocytotoxic activity of complex **3** cannot be delineated from the cellular uptake measurements. Moreover, it has been reported that Re(I) carbonyl complexes bearing sulfonic acid groups on polypyridyl ligand were found to be uptaken by phagocytosis and localized into digestive vacuoles which lowered their cytotoxicity considerably.[60] A similar effect cannot be ruled out in our case considering the nature of complex **3** similar to the Re(I) species. Another interesting observation from these studies is the nearly similar extent of cellular uptake for the [FeL(dpq)] and complex **1**, but a widely different response was observed in the photocytotoxicity studies. [FeL(dpq)] neither shows dark toxicity, nor photocytotoxicity, whereas complex **1** shows low dark toxicity and significant photocytotoxicity on irradiation with visible light which might perhaps result from a faster rate of metabolism of [FeL(dpq)] compared to [FeL(dpqC)] (**1**).

DAPI Staining. The nuclear morphology and cell-death mechanism in HeLa induced by the highly photocytotoxic complex **5** were investigated by nuclear staining with DAPI 2 h

dx.doi.org/10.1021/ic1024229 |*Inorg. Chem.* 2011, 50, 2975–2987

after visible light phototreatment (Figure 6). The untreated cells with intact cell membrane showed very poor uptake of the nuclear stain, whereas the cells treated with complex **5** (2 μM) underwent drastic change in cell morphology with rounding up from its normal spindle-shape with concomitant loss in cell−cell contact. Nuclear staining showed that some of the cells have chromatin concentrated around the nuclear periphery while some cells displayed aggregated and smeared chromatin. Such nuclear features signify DNA breakdown which has been induced directly or indirectly upon phototreatment in presence of complex **5**. Moreover, such DNA degradation is usually encountered in apoptotic cells. Thus we may conclude that complex **5** induces cell death in HeLa through an apoptotic pathway. Apoptosis was also found to be induced very rapidly which is a hallmark of photodynamic cell killing.

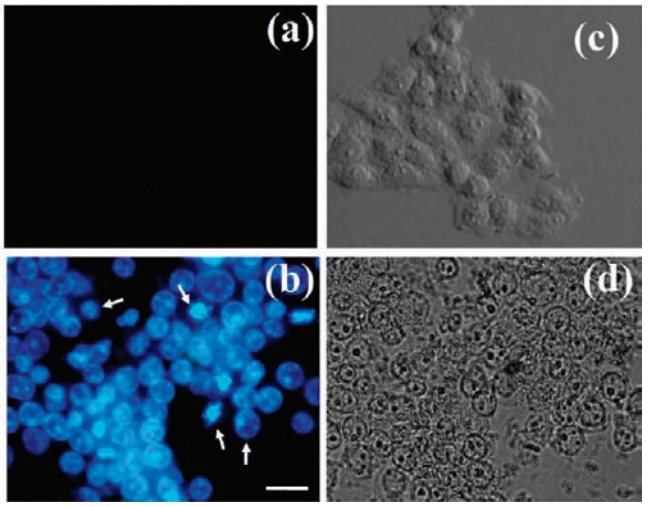

Figure 6. DAPI staining of HeLa cells treated with complex **5** for 4 h in dark followed by photoexposure to visible light (400−700 nm, 10 $J\,cm^{-2}$). The images were acquired 2 h after photoexposure. Panels (a) and (b) are the fluorescence images (acquired with 360/20 nm excitation filter and 460/40 emission filter) of control and treated cells (DAPI stained). Panels (c) and (d) represent their corresponding bright field images. The scale bar is 25 μm.

Computational Studies. Insights into the electronic structures of the iron(III) complexes were made to account for the wide photochemical behavior *in vitro*. The optimized geometries of the complexes were obtained from the crystal structure of complex **6** (Supporting Information, Figures S25−S29).[21] We have used β molecular orbitals throughout our analysis. A detailed analysis of the highest occupied molecular orbitals (HOMOs) and lowest unoccupied molecular orbitals (LUMOs) of complex **6** are listed in Table 5 where orbital energies and compositions are listed. A correlation diagram of the molecular orbitals among the iron(III) complexes **2**, **4**, **5**, and **6** was made to examine the variation of relative energies of the HOMOs and LUMOs in these complexes (Figure 7). The HOMOs and LUMOs of these

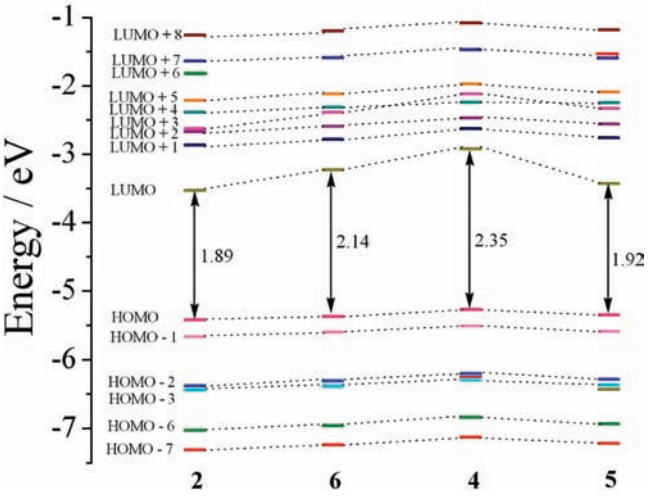

Figure 7. Comparison among the frontier orbitals of the complexes **2**, **4**, **5**, and **6**. Results obtained at UB3LYP/(6-311G for C, H, N, and O and def2-TZVP for Fe) level of theory.

Table 5. Energies (eV) and Composition of HOMOs and LUMOs of Complex 2 [FeL(dppzc)][a]

MO	*E*	Composition
LUMO + 8	−1.26	$3d_{z^2}$ (Fe), $3d_{xz}$ (Fe), $3d_{yz}$ (Fe), $3d_{xy}$ (Fe)
LUMO + 7	−1.64	$3d_{xy}$ (Fe), $3d_{xz}$ (Fe), $3d_{x^2-y^2}$ (Fe)
LUMO + 6	−1.81	π^* (dppzc), $3d_{xy}$ (Fe)
LUMO + 5	−2.21	$3d_{z^2}$ (Fe), $3d_{xz}$ (Fe), $3d_{xy}$ (Fe), π^* (bipyridyl unit)
LUMO + 4	−2.39	$3d_{yz}$ (Fe), $3d_{xz}$ (Fe), $3d_{x^2-y^2}$ (Fe), $2p_z$ (O2),[b] $2p_z$ (O3)[b]
LUMO + 3	−2.63	$3d_{x^2-y^2}$ (Fe), $3d_{yz}$ (Fe), π^* (dppzc)
LUMO + 2	−2.67	$3d_{yz}$ (Fe), $3d_{x^2-y^2}$ (Fe), π^* (dppzc)
LUMO + 1	−2.87	$3d_{z^2}$ (Fe), $3d_{xz}$ (Fe), $3d_{yz}$ (Fe), π^* (bipyridyl unit)
LUMO	−3.53	π^* (phenazine unit)
HOMO	−5.42	$2p_x$ (O2), $[2p_x + 2p_z]$ (O3), π (phenolate)
HOMO − 1	−5.67	$2p_x$ (O2), π (phenolate)
HOMO − 2	−6.38	$[2p_x + 2p_y]$(O6)[c]
HOMO − 3	−6.44	π (phenolate)
HOMO − 6	−7.03	$[2p_z - 2p_x]$ (O2), $3d_{xz}$ (Fe), $3d_{yz}$ (Fe), $[2p_z - 2p_x]$(N9)[d]
HOMO − 7	−7.31	$[2p_z - 2p_y]$ (O3), $2p_z$ (O2), p_x (O5), $3d_{xy}$ (Fe)
HOMO − 8	−7.37	π (dppzc)

[a] Complex calculated at UB3LYP/(6-311G for C, H, N, O and Def2-TZVP for Fe) level of theory. [b] O2 and O3 are the two phenolate oxygen atoms. [c] O6 is the oxygen atom in the C═O moiety. [d] N9 is the N-atom of the ligand L.

dx.doi.org/10.1021/ic1024229 |*Inorg. Chem.* 2011, 50, 2975–2987

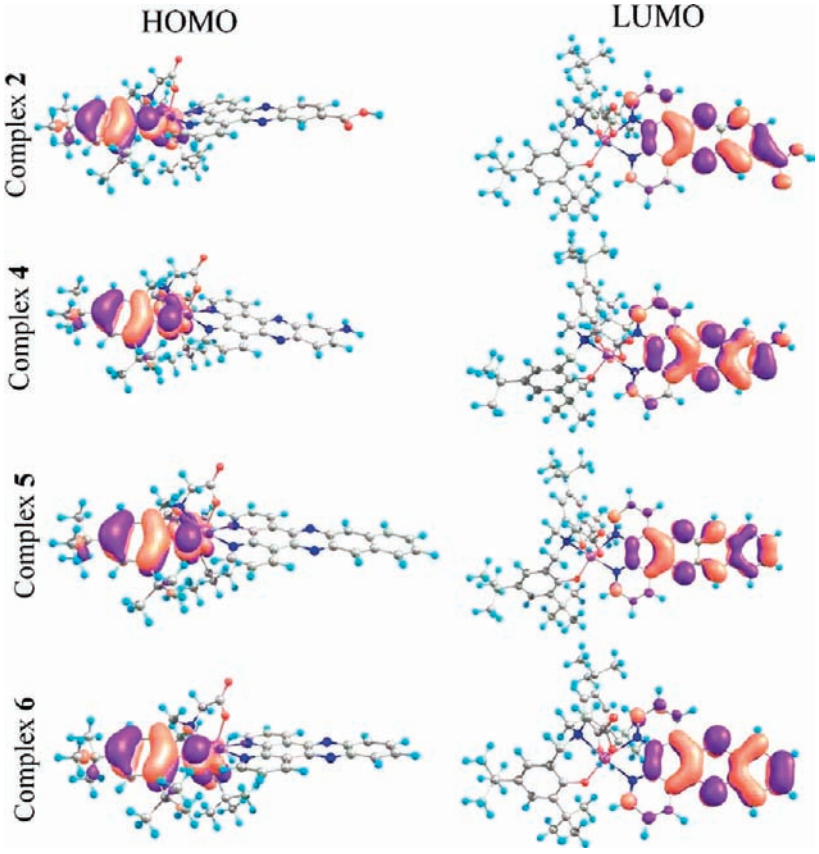

Figure 8. Schematic representation of the HOMOs and LUMOs of the complexes **2**, **4**, **5**, and **6**.

complexes are shown in Figure 8. From the correlation diagram it is observed that the nature of HOMOs and LUMOs does not change much while going from complex **2** to **6** to **4** to **5**. For all the complexes, the first three HOMOs, namely, HOMO, HOMO−1, and HOMO−2, are predominantly constructed by the 2p orbitals of the phenolate oxygen atoms and hence the substituents on the dppz ligands do not affect the energies of the HOMOs significantly (0.05 eV). On the other hand, the LUMOs of these four complexes have an antibonding π-character situated on the phenazine unit and hence the energies are significantly affected by the substituents on the phenazine ring. On going from complex **2** to complex **6**, the LUMO is destabilized by 0.3 eV, with similar destabilization being observed while going from **6** to **4**. The net result is the increase in HOMO−LUMO gap (complex **2**: 1.89 eV; complex **6**: 2.14 eV; complex **4**: 2.35 eV) with the addition of more electron donating substituent at the phenazine unit of the bidentate ligand. For complex **5**, the LUMO is stabilized ($E_{LUMO-HOMO}$ = 1.92 eV) because of the presence of extended conjugation arising from the additional phenyl ring in the phenazine unit. Except for HOMO−3, which is mainly of π−character (phenolate), the other two lower lying HOMOs (HOMO−6 and HOMO−7) are mainly composed of the 2p orbitals of the phenolate oxygen atoms with little contribution from the iron d-orbitals. All the higher lying LUMOs (LUMO+1 to LUMO+5, LUMO+7 and LUMO+8), except LUMO+3, is largely of Fe 3d character. LUMO+3 has a significant contribution from the π^* orbital of dppzc ligand and hence is destabilized by the introduction of electron-donating substituent on the phenazine unit. The LUMOs which are mainly concentrated on the iron(III) 3d-orbitals play an important role in the photochemical reactions as photoexcitation of the electrons from the HOMOs to these LUMOs could lead to an excited state which might have a pivotal role in the reduction of iron(III) to iron(II).

TD-DFT calculations have been performed to investigate the photochemical properties for the iron(III) complexes **2**, **4**, **5**, and **6**. The major optical transitions above 400 nm with an oscillator strength $f > 0.005$ are tabulated in Supporting Information, Tables S1−S4. Complex **2** exhibits two large transitions at 587 and 560 nm with oscillator strengths of 0.0634 and 0.0204, respectively. The final state of these transitions is LUMO+4 which is composed of the 3d orbitals of the iron atom, and the initial states are the orbitals concentrated on the oxygen atom of the phenolate moieties (HOMO and HOMO−1). Therefore we assign this band as a LMCT band. Similar kind of LMCT bands are observed for the other complexes as well. These transitions can generate excited states which may lead to the reduction of Fe(III) to Fe(II) as proposed earlier. The next two high intensity transitions appear at the 445−437 nm region for all the complexes. These two bands originate from the excitation of electrons from the HOMOs (HOMO, HOMO−2, and HOMO−6) which are composed of 2p orbitals of phenolate oxygen atom to the LUMOs (LUMO+1, LUMO+2, and LUMO+6) which have predominantly metal 3d orbital character. Therefore these two transitions are also of LMCT type. A peak at 488 nm has also been observed for complex **5** for which the final state is LUMO and the initial states are HOMO−3 and HOMO−4 that are π-MOs localized on the dppn ligand. We, therefore, assign it as an ILCT transition. An intense transition has been observed only for complex **4** at 423 nm because of the appearance of a π-MO as HOMO−3 which involves an intraligand charge transfer (ILCT)

dx.doi.org/10.1021/ic1024229 |*Inorg. Chem.* 2011, 50, 2975–2987

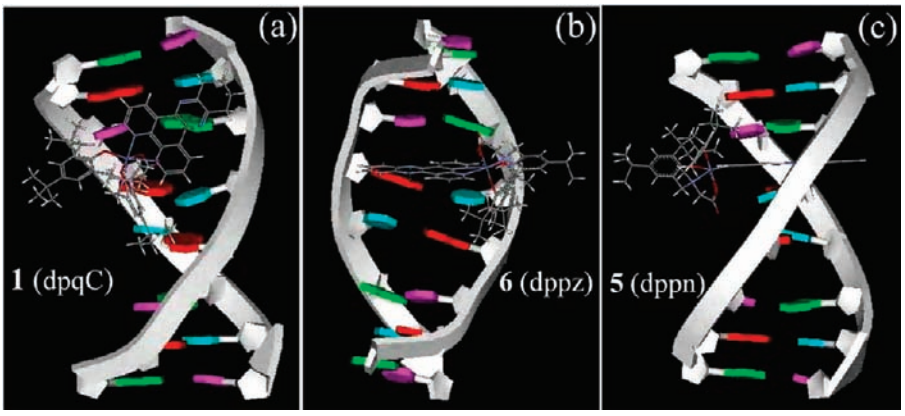

Figure 9. View of the energy minimized docked structure of [FeL(dpqC)] (**1**) (a), [FeL(dppz)] (**6**) (b), and [FeL(dppn)] (**5**) (c) with $d(GACATGTC)_2$.

(HOMO−3 to LUMO) transition. Another high intensity transition is observed for all the complexes in 415 nm region. This transition involves excitation from low lying HOMOs such as HOMO−5, HOMO−6, and HOMO−8 to the metal-based LUMOs like LUMO+1, LUMO+2, and LUMO+4.

Molecular docking calculations were carried out to gain insights into the binding properties of the substituted dppz iron(III) complexes with DNA and to obtain the energy minimized docked structures (Figure 9, Supporting Information, Figure S30). The calculations were carried out with the complexes **1**−**6** and $d(GACATGTC)_2$ with GOLD suite. Complex **6**, in agreement with the experimental data, was found to partially intercalate with DNA along the major groove. Complex **1** was also found to interact with DNA through the major groove, but no intercalation was observed in this case. Complex **5** with dppn as the bidentate ligand showed an intercalative mode of binding which supports its high binding affinity toward DNA. Although complexes **2** and **4** displayed intercalative mode of binding with DNA, complex **4** was found to possess additional hydrogen bonding interaction between the phosphate backbone and the terminal amine group on the dppz ring. This hydrogen bonding interaction might play a pivotal role in the enhanced binding constant of complex **4** as compared to complex **6**. Complex **3** was observed to interact along the major groove of DNA, but no intercalative binding was observed in this case. This is possibly due to the steric bulk of the sulfonic acid group on the dppz ring. The binding energies of the lowest energy docked structures are tabulated in Supporting Information, Table S5, and the hydrogen bonding interactions are given in Supporting Information, Tables S6−S11. The docking calculations thus agree well with our experimentally observed binding properties.

CONCLUSIONS

We have synthesized five new iron(III) complexes having a tetradentate phenolate based ligand and bidentate photosensitizing modified dipyridophenazine ligands to study the structure−activity relationship (SAR) of the complexes with respect to photonucleolytic and photocytotoxic properties. Complexes **1**−**5** are excellent binders to double helical DNA with the dppn complex **5** showing a high binding constant value of $\sim 10^6\ M^{-1}$. The visible light-induced DNA cleavage property of the complexes shows direct correlation with the DNA binding propensities, and photocleavage of DNA proceeds via a photoredox pathway generating hydroxyl radicals. Photocytotoxicity experiments on HeLa cells demonstrate that the complexes with electron-donating group (**4**), cyclohexyl (**1**), or extended aromatic moiety (**5**) are highly photoactive with low dark toxicity. The presence of electron-withdrawing groups indeed lowers the photocytotoxic potential of the complexes. Cellular uptake of the complexes, as determined by ICP-OES, shows an unusual trend in uptake of these complexes with complex **3** being uptaken maximum by the HeLa cells. The rest of the complexes were observed to follow the general trend of lipophilic character to cellular uptake relationship. Taken together our results clearly demonstrate that the activity of photoactive iron(III) complexes can be suitably modulated through tailoring of the dipyridophenazine core. The SAR information available from the present research and rationalized from the computational and DNA docking studies will be used to guide our efforts toward identifying suitable metallodrugs for application in PDT of cancer.

ASSOCIATED CONTENT

Supporting Information. ESI-MS (Figures S1−S5), UV−visible spectra (Figure S6−S9), and cyclic voltammograms (Figures S10−S13), DNA/protein binding and DNA cleavage (Figures S14−S23), MTT assay (Figure S24), energy minimized structures of complexes **1**−**5** (Figures S25−S29), DNA-docked structures (Figure S30), Tables S1−S11 on the theoretical analysis data and experimental details on the binding and cleavage studies and Cartesian coordinates of the energy minimized structures of complexes **1**−**6**. This material is available free of charge via the Internet at http://pubs.acs.org.

AUTHOR INFORMATION

Corresponding Author

*E-mail: jemmis@iisertvm.ac.in (E.D.J., theoretical studies), arc@ipc.iisc.ernet.in (A.R.C., general correspondence). Fax: +91-471-2597442 (E.D.J.), +91-80-23600683 (A.R.C.). Phone: +91-80-471-2597421 (E.D.J.), +91-80-22932533 (A.R.C.).

ACKNOWLEDGMENT

We thank the Department of Science and Technology (DST), Government of India, for the financial support (SR/S5/MBD-02/2007) and ICP-OES facility. We are grateful to the Alexander

von Humboldt Foundation, Germany, for an electrochemical system. D.M. and E.D.J. thank the SERC, Indian Institute of Science, and the CMSD, University of Hyderabad, for computational resources. S.S. thanks CSIR for research fellowship. A.R.C. and E.D.J. thank DST for J. C. Bose National Fellowships.

REFERENCES

(1) Bonnett, R. *Chemical Aspects of Photodynamic Therapy*; Gordon & Breach: London, U.K., 2000.
(2) (a) Detty, M. R.; Gibson, S. L.; Wagner, S. J. *J. Med. Chem.* **2004**, *47*, 3897–3915. (b) Delaey, E.; Van Laar, F.; De Vos, D.; Kamuhabwa, A.; Jacobs, P.; De Witte, P. *J. Photochem. Photobiol., B* **2000** *55*, 27–36.
(3) Wheate, N. J.; Walker, S.; Craig, G. E.; Oun, R. *Dalton Trans.* **2010**, *39*, 8113–8127.
(4) (a) Dhar, S.; Liu, Z.; Thomale, J.; Dai, H.; Lippard, S. J. *J. Am. Chem. Soc.* **2008**, *130*, 11467–11476. (b) Mackay, F. S.; Woods, J. A.; Heringová, P.; Kašpárková, J.; Pizarro, A. M.; Moggach, S. A.; Parsons, S.; Brabec, V.; Sadler, P. J. *Proc. Natl. Acad. Sci. U.S.A.* **2007**, *104*, 20743–20748.
(5) Pandey, R. K.; Potter, W. R.; Meunier, I.; Sumlin, A. B.; Smith, K. M. *Photochem. Photobiol.* **1995**, *62*, 764–768.
(6) Allen, C. M.; Langlois, R.; Sherman, W. M.; Madeleine, C. L.; Van Lier, J. E. *Photochem. Photobiol.* **2002**, *76*, 208–216.
(7) Evenson, J. F.; Sommer, S.; Rimington, C.; Moan, J. *Br. J. Cancer* **1987**, *55*, 483–486.
(8) Pandey, R. K.; Sumlin, A. B.; Potter, W. R.; Bellnier, D. A.; Henderson, B. W.; Constantine, S.; Aoudia, M.; Rodgers, M. A. J.; Smith, K. M.; Dougherty, T. J. *Photochem. Photobiol.* **1996**, *63*, 194–205.
(9) Henderson, B. W.; Bellnier, D. A.; Graco, W. R.; Sharma, A.; Pandey, R. K.; Vaughan, L.; Weishaupt, K. R.; Rodgers, M. A. J.; Dougherty, T. J. *Cancer Res.* **1997**, *57*, 4000–4007.
(10) Zheng, G.; Potter, W. R.; Camacho, S. H.; Missert, J. R.; Wang, G.; Bellnier, D. A.; Henderson, B. W.; Rodgers, M. A. J.; Dougherty, T. J.; Pandey, R. K. *J. Med. Chem.* **2001**, *44*, 1540–1559.
(11) Chen, Y.; Graham, A.; Potter, W.; Morgan, J.; Vaughan, L.; Bellnier, D. A.; Henderson, B. W.; Oseroff, A.; Dougherty, T. J.; Pandey, R. K. *J. Med. Chem.* **2002**, *45*, 255–258.
(12) Castanoa, A. P.; Demidova, T. N.; Hamblin, M. R. *Photodiag. Photodyn. Ther.* **2004**, *1*, 279–293.
(13) Castanoa, A. P.; Demidova, T. N.; Hamblin, M. R. *Photodiag. Photodyn. Ther.* **2005**, *2*, 1–23.
(14) Margaron, P.; Gregoire, M.; Scasnar, V. *Photochem. Photobiol.* **1996**, *63*, 217–223.
(15) Boyle, R. W.; Dolphin, D. *Photochem. Photobiol.* **1996**, *63*, 469–485.
(16) Smith, G. J. *Photochem. Photobiol.* **1985**, *41*, 123–126.
(17) Angeles-Boza, A. M.; Chifotides, H. T.; Aguirre, J. D.; Chouai, A.; Fu, P. K.-L.; Dunbar, K. R.; Turro, C. *J. Med. Chem.* **2006**, *49*, 6841–6847.
(18) Harlos, M.; Ott, I.; Gust, R.; Alborzinia, H.; Wölfl, S.; Kromm, A.; Sheldrick, W. S. *J. Med. Chem.* **2008**, *51*, 3924–3933.
(19) Schäfer, S.; Ott, I.; Gust, R.; Sheldrick, W. S. *Eur. J. Inorg. Chem.* **2007**, 3034–3046.
(20) Scharwitz, M.; Ott, I.; Geldmacher, Y.; Gust, R.; Sheldrick, W. S. *J. Organomet. Chem.* **2008**, *693*, 2299–2309.
(21) Saha, S.; Majumdar, R.; Roy, M.; Dighe, R. R.; Chakravarty, A. R. *Inorg. Chem.* **2009**, *48*, 2652–2663.
(22) Perrin, D. D.; Armarego, W. L. F.; Perrin, D. R. *Purification of Laboratory Chemicals*; Pergamon Press: Oxford, 1980.
(23) Delaney, S.; Pascaly, M.; Bhattacharya, P. K.; Han, K.; Barton, J. K. *Inorg. Chem.* **2002**, *41*, 1966–1974.
(24) da Silva Miranda, F.; Signori, A. M.; Vicente, J.; de Souza, B.; Priebe, J.; Szpoganicz, B.; Goncalves, N. S.; Neves, A. *Tetrahedron* **2008**, *64*, 5410–5415.
(25) Gholamkhass, B.; Koike, K.; Negishi, N.; Hori, H.; Takeuchi, K. *Inorg. Chem.* **2001**, *40*, 756–765.
(26) Yam, V. W.-W.; Lo, K. K.-W.; Cheung, K.-K.; Kong, R. Y.-C. *J. Chem. Soc., Chem. Commun.* **1995**, 1191–1193.
(27) Choi, C.-S.; Mutai, T.; Arita, S.; Araki, K. *J. Chem. Soc., Perkin Trans. 2* **2000**, 243–247.
(28) Wilson, J. G. *Aust. J. Chem.* **1990**, *43*, 1283–1289.
(29) Kahn, O. *Molecular Magnetism*; VCH: Weinheim, 1993.
(30) Reichman, M. E.; Rice, S. A.; Thomas, C. A.; Doty, P. *J. Am. Chem. Soc.* **1954**, *76*, 3047–3053.
(31) McGhee, J. D.; von Hippel, P. H. *J. Mol. Biol.* **1974**, *86*, 469–489.
(32) Carter, M. T.; Rodriguez, M.; Bard, A. J. *J. Am. Chem. Soc.* **1989**, *111*, 8901–8911.
(33) Waring, M. *J. Mol. Biol.* **1965**, *13*, 269–282.
(34) LePecq, J.-B.; Paoletti, C. *J. Mol. Biol.* **1967**, *27*, 87–106.
(35) Lee, M.; Rhodes, A. L.; Wyatt, M. D.; Forrow, S.; Hartley, J. A. *Biochemistry* **1993**, *32*, 4237–4245.
(36) Quiming, N. S.; Vergel, R. B.; Nicolas, M. G.; Villanueva, J. A. *J. Health Sci.* **2005**, *51*, 8–15.
(37) Bernadou, J.; Pratviel, G.; Bennis, F.; Girardet, M.; Meunier, B. *Biochemistry* **1989**, *28*, 7268–7275.
(38) Mosmann, T. *J. Immunol. Methods* **1983**, *65*, 55–63.
(39) Holzer, A. K.; Samimi, G.; Katano, K.; Naerdemann, W.; Lin, X.; Safaei, R.; Howell, S. B. *Mol. Pharmacol.* **2004**, *66*, 817–823.
(40) Sasmal, P. K.; Saha, S.; Majumdar, R.; Dighe, R. R.; Chakravarty, A. R. *Chem. Commun.* **2009**, 1703–1705.
(41) (a) Frisch, M. J.; et al. *Gaussian 03*, revision C.02; Gaussian, Inc.: Wallingford, CT, 2004. (b) Frisch, M. J.; et al. *Gaussian 09*, Revision A.02; Gaussian, Inc.: Wallingford, CT, 2009.
(42) (a) Hehre, W.; Radom, L.; Schleyer, P. v. R.; Pople, J. A. *Ab Initio Molecular Orbital Theory*; Wiley: New York, 1986. (b) Becke, A. D. *J. Chem. Phys.* **1993**, *98*, 5648–5652. (c) Becke, A. D. *Phys. Rev. A* **1988**, *38*, 3098–3100. (d) Lee, C.; Yang, W.; Parr, R. G. *Phys. Rev. B* **1988**, *37*, 785–789. (e) Vosko, S. H.; Wilk, L.; Nusair, M. *Can J. Phys.* **1980**, *58*, 1200–1211.
(43) Schäfer, A.; Huber, C.; Ahlrichs, R. *J. Chem. Phys.* **1994**, *100*, 5829–5835.
(44) Reed, A. E.; Curtiss, L. A.; Weinhold, F. *Chem. Rev.* **1988**, *88*, 899–926.
(45) Jones, G.; Willett, P.; Glen, R. C.; Leach, A. R.; Taylor, R. *J. Mol. Biol.* **1997**, *267*, 727–748.
(46) (a) Drain, C. M.; Christensen, B.; Mauzerall, D. C. *Proc. Natl. Acad. Sci. U.S.A.* **1989**, *86*, 6959–6962. (b) Drain, C. M.; Mauzerall, D. C. *Biophys. J.* **1992**, *63*, 1556–1563.
(47) Shongwe, M. S.; Kaschula, C. H.; Adsetts, M. S.; Ainscough, E. W.; Brodie, A. M.; Morris, M. J. *Inorg. Chem.* **2005**, *44*, 3070–3079.
(48) Toshima, K.; Takano, R.; Ozawa, T.; Matsumura, S. *Chem. Commun.* **2002**, 212–213.
(49) Ramaiah, D.; Eckert, I.; Arun, K. T.; Weidenfeller, L.; Epe, B. *Photochem. Photobiol.* **2002**, *76*, 672–677.
(50) Olmsted, J.; Kearns, D. R. *Biochemistry* **1977**, *16*, 3647–3654.
(51) Joyce, L. E.; Aguirre, J. D.; Angeles-Boza, A. M.; Chouai, A.; Fu, P. K.-L.; Dunbar, K. R.; Turro, C. *Inorg. Chem.* **2010**, *49*, 5371–5376.
(52) Ascoli, G. A.; Domenici, E.; Bertucci, C. *Chirality* **2006**, *18*, 667–679.
(53) Khan, A. U. *J. Phys. Chem.* **1976**, *80*, 2219–2227.
(54) Lahiri, D.; Bhowmick, T.; Pathak, B.; Shameema, O.; Patra, A. K.; Ramakumar, S.; Chakravarty, A. R. *Inorg. Chem.* **2009**, *48*, 339–349.
(55) Barbeau, K. *Photochem. Photobiol.* **2006**, *82*, 1505–1516.
(56) Maurer, D.; Kraft, B. J.; Lato, S. M.; Ellington, A. D.; Zaleski, J. M. *Chem. Commun.* **2000**, 69–70.
(57) Zhao, R.; Hammitt, R.; Thummel, R. P.; Liu, Y.; Turro, C.; Snapka, R. M. *Dalton. Trans.* **2009**, 10926–10931.
(58) Fernández-Moreira, V.; Thorp-Greenwood, F. L.; Coogan, M. P. *Chem. Commun.* **2010**, 186–202.

(59) (a) Williams, P. G.; Helmer, M. A.; Wright, L. C.; Dyne, M.; Fox, R. M.; Holmes, K. T.; May, G. L.; Mountford, C. E. *FEBS Lett.* **1985**, *192*, 159–164. (b) Le, T. T.; Huff, T. B.; Cheng, J.−X. *BMC Cancer* **2009**, *9*, 42–56.

(60) Amoroso, A. J.; Coogan, M. P.; Dunne, J. E.; Fernández-Moreira, V.; Hess, J. B.; Hayes, A. J.; Lloyd, D.; Millet, C.; Pope, S. J. A.; Williams, C. *Chem. Commun.* **2007**, 3066–3068.